

***DETECTION OF SUPERCOOLED LIQUID IN MIXED-PHASE CLOUDS  
USING RADAR DOPPLER SPECTRA***

E. P. Luke<sup>1</sup>, P. Kollias<sup>2</sup>, and M. D. Shupe<sup>3</sup>

<sup>1</sup> Atmospheric Sciences Division, Brookhaven National Laboratory, Upton, NY.

<sup>2</sup> Department of Atmospheric and Oceanic Sciences, McGill University, Montreal, Quebec.

<sup>3</sup> Cooperative Institute for Research in Environmental Sciences, University of Colorado and NOAA, Boulder, CO.

Corresponding author: Edward P. Luke, Atmospheric Sciences Division, Brookhaven National Laboratory, Bldg 490D, Upton, NY, 11973; Email: eluke@bnl.gov

Submitted to  
*Journal of Geophysical Research - Atmospheres*

July 2009

**Environmental Sciences Department/Atmospheric Sciences Division**

**Brookhaven National Laboratory**

P.O. Box 5000

Upton, NY 11973-5000

www.bnl.gov

Notice: This manuscript has been authored by employees of Brookhaven Science Associates, LLC under Contract No. DE-AC02-98CH10886 with the U.S. Department of Energy. The publisher by accepting the manuscript for publication acknowledges that the United States Government retains a non-exclusive, paid-up, irrevocable, world-wide license to publish or reproduce the published form of this manuscript, or allow others to do so, for United States Government purposes.

This preprint is intended for publication in a journal or proceedings. Since changes may be made before publication, it may not be cited or reproduced without the author's permission.

## **DISCLAIMER**

This report was prepared as an account of work sponsored by an agency of the United States Government. Neither the United States Government nor any agency thereof, nor any of their employees, nor any of their contractors, subcontractors, or their employees, makes any warranty, express or implied, or assumes any legal liability or responsibility for the accuracy, completeness, or any third party's use or the results of such use of any information, apparatus, product, or process disclosed, or represents that its use would not infringe privately owned rights. Reference herein to any specific commercial product, process, or service by trade name, trademark, manufacturer, or otherwise, does not necessarily constitute or imply its endorsement, recommendation, or favoring by the United States Government or any agency thereof or its contractors or subcontractors. The views and opinions of authors expressed herein do not necessarily state or reflect those of the United States Government or any agency thereof.

## **Abstract**

Cloud phase identification from active remote sensors is challenging, especially in the temperature range from 0 to -40 °C, where both liquid and ice hydrometeor phases are sustainable. Millimeter wavelength cloud radars (MMCR) are able to penetrate and detect multiple cloud layers. However in mixed-phase conditions, ice crystals dominate the radar signal, rendering the detection of liquid droplets from radar observables more difficult. The technique proposed here overcomes this fundamental limitation by using morphological features in MMCR Doppler spectra to detect supercooled liquid droplets in the radar sampling volume in the presence of ice particles. High lidar backscatter and near-zero lidar depolarization measurements - good indicators of the presence of liquid droplets - from the Mixed-Phase Arctic Clouds Experiment (MPACE) conducted in Barrow, Alaska, are used to evaluate the potential of the technique to detect mixed-phase conditions. Due to the ability of MMCRs to penetrate multiple liquid layers, this radar-based technique does not suffer from the extinction limitations of lidars and is thus able to expand cloud phase identification methods to cloud regions beyond where lidars can penetrate, providing output at the native radar resolution. The technique is applicable to all profiling radars that have sufficient sensitivity to observe the small amount of liquid in mixed-phase clouds.

## 1. INTRODUCTION

The life cycles and radiative properties of clouds are highly sensitive to the phase of their hydrometeors (i.e., liquid or ice). Knowledge of cloud phase is essential for specifying the optical properties of clouds. Current cloud parameterizations that partition water into liquid and ice based on temperature are characterized by large uncertainties (Curry et al., 1986; Hobbs and Rangno, 1985; Intrieri et al., 2002). These uncertainties are particularly important in high geographical latitudes and temperature ranges where both liquid droplets and ice crystals can coexist (mixed-phase cloud). Furthermore, the presence of both ice and liquid affects the macroscopic properties of clouds including their propensity to precipitate.

Mixed-phase clouds have a major presence in global cloud cover. Cloud type classifications made at the ARM North Slope of Alaska (NSA) observation site over the past six years and similar results from the year-long Surface Heat Budget of the Arctic (SHEBA) project have shown that mixed-phase clouds occur approximately 45% of the time in the Arctic (Shupe et al. 2006) with maximum occurrence during the spring and fall transition seasons. These Arctic mixed-phase clouds are typically stratiform in nature, occur at the top of the inversion-capped boundary layer, often contain little liquid water, and are remarkably persistent (sometimes lasting for days to weeks). A preliminary perusal of radar measurements from the ARM Southern Great Plains (SGP) observation site during the winter of 2003/2004 has suggested that mixed-phase clouds occurred on about 40% of the days during the months of November through March. These clouds were most frequently observed above the boundary layer and typically lasted for a few

hours. In spite of the macroscopic differences between the mixed-phase clouds at these two sites, they are both important for a variety of reasons. In the Arctic, the liquid water found in mixed-phase clouds, even in the cold Polar winter, has been shown to play the dominant role in cloud-surface radiative interactions (Shupe and Intrieri 2004), and can have profound impacts on the start and duration of the melt season, the total extent and thickness of sea-ice, and indirectly on the annual evolution of the surface albedo (e.g., Zhang et al. 1996, Maykut and Untersteiner 1971). In the mid-latitudes, in addition to radiative implications, mixed-phase clouds also have great importance with respect to aircraft icing hazards (Cober et al. 2001).

Despite their importance, mixed-phase clouds are severely understudied compared to arguably simpler single-phase clouds. In-situ measurements in mixed-phase clouds are hindered due to aircraft icing hazards, difficulties distinguishing hydrometeor phase, and discrepancies in methods for deriving physical quantities (Wendisch et al. 1996, Lawson et al. 2001). Satellite-based retrievals of cloud phase in high latitudes are often hindered by the highly reflecting ice-covered ground and persistent temperature inversions.

In this study, we use measurements from the US Department of Energy (DOE) Atmospheric Radiation Measurement (ARM) program Mixed-Phase Arctic Clouds Experiment (MPACE, Verlinde et al., 2007) conducted in the fall of 2004 at the North Slope of Alaska (NSA) site (e.g., Ackerman and Stokes, 2003). During the experiment, collocated measurements from the University of Wisconsin High Spectral Resolution Lidar (HSRL, Eloranta, 2005) and the ARM program millimeter-wavelength cloud radar (MMCR, Moran et al., 1998) were collected. Prior to MPACE, the NSA MMCR receiver

was upgraded (Kollias et al., 2007) and continuous recording of the MMCR Doppler spectra was available. The MMCR Doppler spectrum reports the full distribution of the return echo over a range of Doppler velocities and thus provides detailed information about cloud microphysics and dynamics (e.g., Kollias et al., 2002; Luke et al., 2007). Before the upgrade, only the first three moments of the Doppler spectrum were recorded, namely the zeroth moment or radar reflectivity, the first moment or mean Doppler velocity and the second moment or Doppler spectrum width. These three moments of the Doppler spectrum are sufficient to describe the spectrum shape if it does not deviate significantly from the Gaussian distribution (moment approach). In mixed-phase conditions, the moments are dominated by the ice crystals' characteristics and the detection of supercooled liquid is very difficult.

Our objective is to demonstrate that we can overcome the inability of the radar moment approach to detect the presence of supercooled liquid in mixed-phase conditions through careful analysis of recorded Doppler spectra from the vertically pointing radars of the ARM program (spectral approach). Our technique looks beyond the traditional moment approach in the analysis of cloud radar observations and attempts to retrieve microphysical properties from the typically skewed, often multi-modal, and sometimes very complex morphologies of cloud radar Doppler spectra (Kollias et al., 2007a). These distortions result from the interplay of cloud dynamics, microphysics and cloud phase. We decompose the Doppler spectra into several bands of differing resolution each localized in Doppler velocity using continuous wavelet transforms and analyze the resulting patterns with a neural network.

Since we do not have direct measurements of the spatial distribution of liquid in the atmospheric column, we use the next best available proxy, collocated measurements of lidar backscatter ( $\beta$ ) and circular depolarization (CDR) to train and validate our retrieval algorithm. Additional validation (but not algorithm training) is provided by integrated liquid water path measurements from a collocated microwave radiometer. First, we demonstrate that the radar-based retrieval technique accurately predicts the presence of supercooled liquid in mixed-phase clouds using the radar Doppler spectra as the only input. Second, we demonstrate that the technique is capable of predicting with reasonable success the lidar signals ( $\beta$  and CDR) from the Doppler spectra.

## **2. BACKGROUND**

From the ground, the retrieval of mixed-phase cloud properties has been the subject of extensive research over the past 20 years using polarization lidars (e.g., Sassen et al. 1990), dual radar wavelengths (e.g., Gosset and Sauvageot 1992; Sekelsky and McIntosh, 1996), and recently, radar Doppler spectra (Shupe et al. 2004, 2008). Millimeter-wavelength radars have substantially improved our ability to observe non-precipitating clouds (Kollias et al., 2007b) due to their superior sensitivity to non-precipitating cloud layers and their ability to penetrate several cloud layers.

In clouds, lidar backscatter  $\beta$  ( $\text{sr}^{-1}\text{m}^{-1}$ ) is proportional to the square of the diameter ( $D$ ) of the hydrometeors ( $\sim D^2$ ). Depolarization of lidar backscatter (circular depolarization ratio, CDR) indicates that the scattering particles are non-spherical. In typical mixed-phase conditions, liquid occurs as a high concentration of small spherical droplets while ice is

distributed in relatively lower concentrations of large, non-spherical ice crystals. As a result, the lidar backscatter ( $\sim D^2$ ) signal is dominated by the high concentration liquid droplets; areas with high intensity lidar backscatter and near-zero lidar depolarization signals indicate the presence of small liquid droplets. On the contrary, the radar backscatter is proportional to the sixth power of the hydrometeor diameter ( $\sigma \sim D^6$ ). Thus in typical mixed-phase conditions, the low concentration large ice crystals dominate the radar backscatter signal which therefore offers little information about the spatial distribution of liquid in the atmospheric column. This is true if only the Doppler moments are available (moments approach). In general, clouds composed of only small liquid droplets do not have a reflectivity higher than -17 dBZ (Frisch et al., 1995). Thus, in subzero temperatures, higher reflectivities suggest the presence of larger particles such as ice crystals. When the conditions of high radar reflectivity (dBZ > -17), high lidar backscatter ( $\beta > 5 \cdot 10^{-5} \text{ sr}^{-1} \text{ m}^{-1}$ ) and near-zero lidar circular depolarization signal (CDR < 0.1) are observed simultaneously, this implies the presence of mixed-phase conditions. Such synergistic cloud phase retrieval schemes that use collocated radar and lidar profiles have been used in the past (e.g., Shupe, 2007). However, synergistic radar/lidar techniques are limited to the maximum height the lidar penetrates before complete signal extinction.

In mixed-phase conditions, at least two particle size distributions (PSD) with different phase, terminal velocity and backscattering characteristics are present in the radar sampling volume. The terminal velocity of cloud droplets is negligible compared to typical vertical motions encountered in clouds, so that where ice crystals are not present the observed mean Doppler velocity is a very good indication of the vertical air motion

(e.g., Kollias et al., 2001, Shupe et al., 2004). In contrast, ice particles have larger and broader fall velocity distributions and account for most of the radar backscattered energy. If sufficient separation between liquid and ice fall velocity distributions exists, the spectra may exhibit a pronounced bi-modality (Fig. 1a) that can be used to retrieve the vertical air motion and liquid and ice microphysics (e.g., liquid water content, ice water content and ice effective radius, Shupe, et. al., 2004). For the MMCR, negative Doppler velocity indicates motion away from the radar (upward). If there is not sufficient separation between liquid and ice fall velocity distributions, then often a skewed mono-modal Doppler spectrum is observed (Fig. 1b). Such asymmetry features in the Doppler spectrum are not captured well using the traditional radar Doppler moments approach and can be a source of information about the presence of mixed-phase conditions.

Cloud turbulence, however, can have an overwhelming effect and smear (smooth) such asymmetries induced by cloud microphysics. Recently, the ARM MMCR's deployed a new optimum sampling strategy, along with continuous recording of the Doppler spectra, which has been specifically designed to minimize the effects of turbulence on the Doppler spectra (Kollias et al., 2007a). These new optimum MMCR sampling settings were operational at the NSA MMCR during the MPACE experiment.

### **3. Extraction of MMCR Doppler Spectra Morphological Features**

Starting with the MMCR Doppler spectra, we remove the noise, eliminate artifacts (e.g., aliasing, spectral images) and identify the significant signal detections from hydrometeors (Kollias et al., 2007a). Then, we apply a second-order Gaussian (Marr)

continuous wavelet transform (CWT) to the spectra (Figs. 2 and 3). The application of the Marr CWT to a Doppler spectrum decomposes the spectral power into a two-dimensional array providing feature localization in both Doppler velocity and width (scale). To demonstrate the ability of the Marr CWT to detect and localize the components of a sum of Gaussians, we applied it to synthetically generated Doppler spectra (Fig. 2). Fig. 2a contains a Gaussian synthetic Doppler spectrum (i.e. unimodal particle size distribution). Fig. 2b contains a synthetic Doppler spectrum generated from a pair of identical Gaussian distributions (i.e. bimodal particle distribution of equal radar reflectivity) resulting in a non-skewed spectrum. Fig. 2c contains a Gaussian pair of unequal magnitude (i.e., liquid and ice particle size distributions), resulting in a skewed spectrum resembling many real spectra. The radar moment approach results in very similar Doppler moments for all three spectra and thus, the subtle differences in the shapes of the three synthetic spectra may not be captured. The operation of the Marr wavelet at a scale appropriate to detect the fundamental Gaussian features on the synthetic spectra is shown in Fig2d-f. The coefficients are different in all three cases, indicating the ability of the Marr wavelet to detect the subtle differences in the shapes of the synthetic Doppler spectra. The wavelet scale appropriate to detect the different particle modes is not known in advance. Thus, we apply the Marr mother wavelet to each recorded MMCR Doppler spectrum at several different scales and use the output as input to a neural network to detect the presence of supercooled liquid in mixed-phase clouds.

Fig. 3 shows the complete set of input parameters to the neural network derived from a typical mixed-phase Doppler spectrum. The observed Doppler spectrum (Fig. 3b) presents evidence of skewness toward the low fall velocity edge of the spectrum due to

the presence of liquid and ice particles in the radar sampling volume. The Marr CWT is applied to the observed Doppler spectrum at 6 different scales (Fig. 3a) and the resulting coefficients (Fig. 3c) are part of the input to the neural network. The radar reflectivity, mean Doppler velocity, spectrum width, skewness, kurtosis, and the left and right slope of the Doppler spectrum significant peak complement the list of input parameters. Parameters such as the radar range (altitude) and temperature are not inputs to the algorithm.

The neural network learns the functional relationship between the input parameters and the presence of supercooled liquid during MPACE by learning to predict the HSRL backscatter and depolarization measurements taken during the same time period. It is known that a neural network can be trained to implement an arbitrary multidimensional functional relationship (e.g., Funahashi 1989) by application of an iterative error minimization technique, such as the backpropagation of errors algorithm (Rumelhart et al., 1986), to a set of representative input and output data. Fig. 4 shows a scatter plot of the actual measured lidar CDR versus the measured lidar backscatter for most of the MPACE field study. We used a small fraction of these HSRL measurements to train the neural network via backpropagation. The boxed area in Fig.4 encloses lidar detections of supercooled liquid (clear separation from solid particle detections). After training, to generate a radar-based supercooled liquid binary mask from new Doppler spectra, the neural network predicts associated values of lidar CDR and backscatter, and a determination is made whether these predicted values fall within this same boxed area.

The training dataset was selected from the first seven days of October 2004. The MMCR

measurements have a vertical resolution of 45 m and temporal resolution of 5 sec. Every seven hours of observations, one hour of MMCR measurements and their corresponding nearest lidar measurements in time and height are selected (Fig. 5). We decided to select training data every seventh hour (the choice of seven is arbitrary) so that the majority of time is not sampled, allowing abundant intervals for testing the predictor's ability to generalize. The selected lidar measurements are divided into two equal-sized groups. One group serves exclusively as the training data source and the other for validation. During each training cycle, the neural network output is evaluated over the validation dataset. Iterations of the network for which an overall improvement occurs are saved. When there is no further improvement after 20,000 cycles, the process terminates.

#### **4. RESULTS**

To validate the performance of our classifier, we first show in detail several retrieved time-height liquid water masks that have good agreement with the independently measured ceilometer cloud base. Next, we show that good agreement between the base of the retrieved liquid mask and the ceilometer cloud base holds for the full month of October 2004. Finally, we demonstrate excellent long-term correlation between time-series of our retrieved liquid mask's column thickness and the integrated liquid water path measured independently by a collocated microwave radiometer. We contrast this with a poor correlation between the total column thickness of significant radar detections and the same time-series of MWR liquid water path. In addition, we demonstrate from soundings that the measured thermodynamic conditions coinciding in time-height with our liquid mask are consistent with mixed-phase conditions.

#### 4.1 Time-Height Liquid Mask Comparisons

The neural network output (prediction of supercooled liquid location via prediction of lidar backscatter and lidar circular depolarization ratio) derived using MMCR Doppler spectra is evaluated with data collected during the ARM MPACE campaign. The first examined case is a deep cloud layer observed on October 7, 2004. Fig. 6 shows the time-height mapping of the MMCR Doppler moments for a one-hour period (10:00-11:00 UTC). This hour is not included in the training dataset. The observed MMCR reflectivities range from -15 to +15 dBZ with distinct streaks of high radar reflectivity originating around 2 km altitude accompanied by increased Doppler velocities. In contrast, the highest Doppler spectrum width values are observed in the layer between 2 and 2.5 km. Interpolated temperature measurements from balloon soundings indicate a near surface temperature of -5 °C and -20 °C near the cloud top. Thus, if liquid is present in the radar echoes, it will be supercooled. It is apparent that from the radar moments it is difficult to infer the cloud phase, although the high radar reflectivity values suggest the presence of ice almost everywhere. The large spectrum width values around 2-2.5 km partially indicate the presence of a particle population with a broad range of velocities and hint at the coexistence of liquid and ice particles; however this is not a firm criterion for the detection of supercooled liquid since localized turbulence can also affect the spectrum width.

A different view of the same cloud is provided by the lidar (Fig. 7). The band of low Circular Depolarization Ratio (CDR) values near the top of the lidar returns is a strong

indication of the presence of spherical particles in the sampled volume. The lidar backscatter measurements for the same period also support this conclusion (Fig. 7b). A band of high backscatter cross-section is present between 1.5 and 2 kilometers, indicating the presence of liquid water that fully attenuates the lidar signal. Four representative spectra from the collocated MMCR are also shown in Fig. 7c corresponding to the indicated times and altitudes of occurrence of Fig. 7b. It is apparent that all four spectra are similar and inseparable on the basis of Doppler moments alone. However, the three spectra coinciding with the band of high lidar backscatter have a subtle skewness or bimodality at their principle peaks' left edge, consistent with the presence of liquid, whereas the fourth (S2) does not.

Using the collocated MMCR Doppler spectra collected during the same period as input to our trained neural network, we predicted the lidar backscatter and CDR, and from these the region containing supercooled liquid (Fig. 8). While our ultimate objective is to retrieve the location of supercooled liquid (Fig. 8c), we also display the predicted lidar backscatter and depolarization. The predicted lidar measurements are directly comparable with the actual lidar observations. The cloud ceiling measured independently (not used as input to the retrieval) by a collocated ceilometer is over-plotted in black. There is excellent morphological consistency between the predicted (Fig. 7a,b) and observed (Fig. 8a,b) lidar backscatter and CDR. The lidar measurements in Fig. 7 do not extend beyond the layer of high backscatter due to extinction of the lidar beam in optically thick cloud; however, more cloud is present up to about four kilometers (Fig. 6). The predicted area of supercooled liquid (Fig. 8c) suggests the presence of a liquid cloud base around 1.8 kilometers and inspection shows the reflectivity at this altitude to be in the range of 0 dB.

Small liquid droplets alone cannot support such high reflectivity values. Furthermore, the MMCR-based detection of supercooled liquid suggests the presence of pockets of liquid near the cloud top (around 4 km height). Lidar measurements are not available to provide verification for the presence of the liquid layer near the cloud top due to complete lidar signal extinction at the first liquid layer. However, the nearest available balloon sounding to the selected period (taken at 11 UTC) indicates the presence of a thin layer with high relative humidity (above 90%) near the cloud top (Fig 9a). Figure 9b shows the temperature profile from the same sounding.

Another one-hour period that demonstrates the potential to detect cloud liquid and predict lidar observables using MMCR Doppler spectra is shown in Figs. 10 and 11. This case is from a multi-liquid layer period with precipitating ice (Fig. 10). The observed lidar CDR and backscatter measurements (Fig. 10a,b) suggest the presence of two liquid layers, but with the upper layer substantially occluded by extinction in the lower layer when compared with the MMCR reflectivity view of the same period (Fig. 10c). The predicted lidar backscatter, CDR and area of supercooled liquid within the range of the radar's operational sensitivity are shown in Fig. 11. Once again, there is remarkable consistency between the observed and predicted lidar backscatter, CDR and location of the supercooled liquid. The independently measured ceilometer cloud base is also shown in Fig. 11. Once again, the sharp liquid base predicted from the neural network coincides very well with the ceilometer cloud base and the high backscatter values measured by the lidar. This figure fills out the picture of two liquid layers, and even suggests a third layer of mixed-phase conditions (Fig. 11c) at 1.2 kilometers which is also briefly hinted in the actual measurements of figure 10a at 6.475 UTC.

## 4.2 Comparisons with Liquid Water Path and Cloud Base Detections

Additional validation of the supercooled liquid detection algorithm is provided through a comparison of our retrieved lowest supercooled liquid layer base and the ceilometer cloud base (Fig. 12a) over the entire month of October 2004. Both time series are smoothed by a box-car window filter of 4 hours duration. The result shows good agreement over this longer time frame, even though training data was only taken from the first week. That our retrieval technique detects not only the presence of supercooled liquid in the column but also accurately locates the base of the first liquid layer is indicative of its sensitivity to detecting small amounts of liquid, since the smallest amounts of liquid are expected at the cloud base level. For comparison, Fig. 12b shows the base of significant radar hydrometeor detections (often the lowest height of the precipitating ice) over the same time period in black, and the ceilometer cloud base in gray. These comparisons clearly demonstrate the method's ability to identify liquid water layers embedded in ice.

The ARM suite of instruments operating at NSA during MPACE included a zenith pointing microwave radiometer providing zenith measurements of integrated liquid water path via its 31.4 GHz channel. The gray curve of Figure 12c shows the recorded liquid water path measured by this instrument over the month of October 2004. The overlaid black curve shows the column thickness of our radar-retrieved liquid mask for the same time period. Liquid mask column thickness and LWP are both smoothed by a box-car window filter of 4 hours duration. The correlation between these two time series is 0.68.

This correlation is expected to be somewhat less than unity due to the natural variability of liquid as a function of height (i.e., differences in liquid water content). For comparison, we generated a time series of the total column thickness of all significant hydrometeor radar detections (liquid and ice), and found its correlation with the MWR liquid water path over the same time period to be only 0.079. We can infer then that the liquid-containing subset of radar returns has been substantially identified within the full set of radar returns over the month-long period. The MWR did not play any role in the training of our algorithm, and thus provides an entirely independent source of validation.

Forty percent of our October 2004 radar-retrieved liquid water mask coincides with radar returns having a reflectivity of at least -15 dBZ (Fig. 13a). When we limit our mask to this higher reflectivity subset, its column thickness correlation with MWR liquid water path actually increases to 0.75. This suggests that mixed-phase clouds dominate the total liquid water present during October 2004 at NSA. For the column thickness of all hydrometeor radar detections of at least -15 dBZ, the correlation with the MWR liquid water path is 0.2. Once again, we can infer the ability of the technique to locate the liquid containing returns within the higher reflectivity ( $> -15$  dBZ) subset.

Figures 13b and c show temperature and relative humidity distributions of interpolated sounding measurements for all time-height pixels identified to contain liquid water that are within one hour of a radiosonde launch during October 2004. The Doppler spectra-based detections of supercooled liquid are found to be within the -30 to 0 °C range. This finding agrees with prevailing theories for the existence of supercooled liquid at temperature ranges of -40 to 0 °C. Another interesting finding is that the bulk of our

supercooled liquid detections occur in areas with relative humidity higher than 90%. Although this is not a surprise, it suggests that future supercooled liquid detection schemes from ground sensors should include the high temporal and spatial resolution sounding information provided at the ARM sites.

## **5. SUMMARY**

The life cycles and radiative properties of clouds are highly sensitive to the phase of their hydrometeors (i.e., liquid or ice). Cloud radars are among the premier instruments used in atmospheric research for the detection of the vertical structure of clouds. Conditional analysis of cloud radar Doppler moments can provide limited information for predicting cloud phase; however, the information is inconclusive in a large fraction of mixed-phase conditions. This limitation comes from dependency of the radar backscatter on the sixth power of the hydrometeor diameter resulting in radar return signals being dominated by the presence of large ice crystals and the masking of the supercooled liquid droplet returns.

Synergistic profiling measurements from cloud radars and lidars have been proposed for the identification of cloud phase based on differences in their scattering mechanisms (e.g., Shupe, 2007). High lidar backscatter and near-zero lidar depolarization measurements have been previously found to correlate very well with the presence of liquid layers in clouds. However, such measurements are not widely available and the detection of supercooled liquid is possible only in areas where a lidar signal is available (subject to liquid attenuation).

The proposed technique overcomes this fundamental limitation of cloud radars and suggests new venues for the retrieval of the location of supercooled liquid using vertically pointing cloud radars. The proposed technique hinges on the idea that careful sampling of clouds by vertically profiling cloud radars (Kollias et al., 2007a) can reduce the detrimental effects of dynamics on the Doppler spectrum morphology. The ARM MMCR's are an example of cloud radars where such sampling is implemented and the recorded Doppler spectra contain microphysical signatures. In this study, we used a wavelet operator on the recorded Doppler spectra in order to identify subtle differences in the Doppler spectrum morphologies that can lead to the detection of the presence of more than one water phase in the radar resolution volume.

Using the MMCR Doppler spectra, we detected the area of supercooled liquid in both single and multi-layer cloud scenes. The retrieved area of the supercooled liquid nicely agrees with the prediction of supercooled liquid from the lidar measurements. A month-long time series of predicted liquid column thickness shows high correlation with integrated liquid water path independently measured by a collocated microwave radiometer. The ability of the MMCR to penetrate multi-layer clouds enables the prediction of lidar observables in areas where lidar measurements are not available due to signal extinction. This extends the ability of ground-based systems to retrieve cloud phase in areas with no lidar measurements and without the use of assumptions related to cloud morphology and spatial distribution of cloud phase.

It is not our intent to suggest that the MMCR could replace the lidar observations. The

suggested technique provides only information about the presence of supercooled liquid in clouds, while lidar measurements help to extract quantitative microphysical information about the cloud droplets and aerosols that are not possible with a cloud radar. Radar sensitivity is another factor that limits the application of the technique. During the ARM MPACE experiment, some physically thin and low-liquid water layers were undetected by the NSA MMCR. Thus, our radar-based technique is applicable only to areas where the liquid radar return is above the detection threshold of the cloud radar. Plans include the application of the technique to all the ARM sites using appropriate training data sets (e.g., micro-pulse and Raman lidar measurements).

The application of wavelets or other operators to the recorded Doppler spectra can lead to new ways of analyzing radar Doppler spectra. Already, the ARM program is producing higher moments of the Doppler spectra (such as skewness and kurtosis) and identifying the presence of spectral multi-modalities. In many cases, these parameters all exhibit good coherence in time and space, and open new venues for process studies in clouds and precipitation using radars.

### **Acknowledgments.**

This research was supported by the Office of Science (BER), U. S. Department of Energy, grant DE-FG02-05ER63965. Data was obtained from the ARM archive and the University of Wisconsin.

## 6. REFERENCES

Ackerman, T. P., and G. Stokes, 2003: The Atmospheric Radiation Measurement program. *Phys. Today*, **56**, 38-45.

Cober, S.G., G.A. Issac, and J.W. Strapp, 2001: Characterization of aircraft icing environments that include supercooled large drops. *J. Appl. Meteor.*, **40**, 1984-2002.

Curry, J. A., 1986: Interactions among turbulence, radiation and microphysics in Arctic stratus clouds. *J. Atmos. Sci.*, **43**, 90-106.

Eloranta, E. W., 2005: High Spectral Resolution Lidar in Lidar: Range-Resolved Optical Remote Sensing of the Atmosphere, K. Weitkamp, ed., Springer-Verlang, New York.

Frisch, A. S., C. W. Fairall, and J. B. Snider, 1995: Measurement of stratus cloud and drizzle parameters in ASTEX with a Ka-band Doppler radar and a microwave radiometer, *J. Atmos. Sci.*, **52**, 2788-2799.

Funahashi K., 1989: On the approximate realization of continuous mappings by neural networks, *Neural Networks*, **2**, pp. 183–192

Gossard E. E., 1994: Measurements of cloud droplet size spectra by doppler radar. *J. Atmos. Oceanic Tech.*, **11**, 712-726

Gosset, M., and H. Sauvageot, 1992: A dual-wavelength radar method for ice-water characterization in mixed-phase clouds. *J. Atmos. Oceanic Technol.*, **9**, 538–547.

Hobbs, P. V., and A. L., Rangno, 1985: Ice particle concentrations in clouds. *J. Atmos. Sci.*, **23**, 2523–2549.

Intrieri, J. M., M. D. Shupe, T. Uttal, and B. J. McCarty, 2002: An annual cycle of Arctic cloud characteristics observed by radar and lidar at SHEBA. *J. Geophys. Res.*, **107**, 8030, doi:10.1029/2000JC000423.

Kollias, P., E.E. Clothiaux, M.A. Miller, E.P. Luke, K.L. Johnson, K.P. Moran, K.B. Widener, and B.A. Albrecht, 2007a: The Atmospheric Radiation Measurement Program cloud profiling radars: Second-generation sampling strategies, processing, and cloud data products. *J. Atmos. Oceanic Technol.*, **24**, 1199–1214.

Kollias, P., E. E. Clothiaux, M. A. Miller, B. A. Albrecht, G. L. Stephens, and T. P. Ackerman, 2007b: Millimeter-wavelength radars – New frontier in atmospheric cloud and precipitation research. *Bull. Amer. Meteor. Soc.*, **88**, 1608–1624.

Kollias, P., B. A. Albrecht, R. Lhermitte, and A. Savtchenko, 2001: Radar observations of updrafts, downdrafts, and turbulence in fair weather cumuli. *J. Atmos. Sci.*, **58**, 1750–1766.

Lawson, P., B. A. Baker, C. G. Schmitt, T. L. Jensen, 2001: An overview of microphysical properties of Arctic clouds observed in May and July 1998 during FIRE ACE. *J. Geophys. Res.*, **106**, 14 989-15 014.

Luke, E. and P. Kollias, A high resolution hydrometeor phase classifier based on analysis of cloud radar Doppler spectra. *American Meteorological Society's 33rd Conference on Radar Meteorology*, Cairns, Australia, August 6-10, 2007.

Moran, K. P., B. E. Martner, M. J. Post, R. A. Kropfli, D. C. Welsh, and K. B. Widener, 1998: An unattended cloud-profiling radar for use in climate research. *Bull. Amer. Meteor. Soc.*, **79**, 443-455.

Maykut, G.A., and N. Untersteiner, 1971: Some results from a time-dependent thermodynamic model of sea ice. *J. Geophys. Res.*, **76**, 1550-1575.

Rumelhart, D.E., G.E. Hinton, and R.J. Williams, 1986: Learning representations by back-propagating errors, *Nature*, **323**, 533 – 536, doi:10.1038/323533a0

Sassen, K., Grund, C.J., Spinhirne, J.D., Hardesty, M.M., and Alvares, J.M., 1990: The 27-28 October 1986 FIRE IFO Case Study: A five lidar overview of cloud structure and evolution. *Mon. Wea. Rev.*, **118**, 2288-2311.

Sekelsky, S. M., and R. E. McIntosh, 1996: Cloud observations with polarimetric 33 GHz and 95 GHz radar. *Meteor. and Atmos. Phys.*, **59**, 123-140.

Shupe, M.D., J.S. Daniel, G. de Boer, E.W. Eloranta, P. Kollias, C.N. Long, E.P. Luke, D.D. Turner, and J. Verlinde, 2008: A Focus On Mixed-Phase Clouds. *Bull. Amer. Meteor. Soc.*, 89, 1549–1562

Shupe, M. D., 2007: A ground-based multiple remote-sensor cloud phase classifier. *Geophys. Res. Lett.*, 34, L22809, doi:10.1029/2007GL031008.

Shupe, M.D., S.Y. Matrosov, and T. Uttal, 2006: Arctic mixed-phase cloud properties derived from surface-based sensors at SHEBA. *J. Atmos. Sci.*, 63, 697-711.

Shupe, M.D., P. Kollias, S.Y. Matrosov, and T.L. Schneider, 2004: Deriving Mixed-Phase Cloud Properties from Doppler Radar Spectra. *J. Atmos. Oceanic Technol.*, **21**, 660–670.

Shupe, M. D., and J. M. Intrieri, 2004: Cloud radiative forcing of the Arctic surface: The influence of cloud properties, surface albedo, and solar zenith angle. *J. Climate*, **17**, 616-628.

Verlinde, H., and Coauthors, 2007: The Mixed-Phase Arctic Cloud Experiment (MPACE). *Bull. Amer. Meteor. Soc.*, **88**, 205 - 221.

Wendisch, M., A. Keil, and A. V. Korolev, 1996: FSSP characterization with monodisperse water droplets. *J. Atmos. Oceanic Technol.*, **13**, 1152-1165.

Zhang, T., K. Stamnes, and S.A. Boxling, 1996: Impact of clouds on surface radiative fluxes and snow melt in the Arctic and subarctic, *J. Climate*, **9**, 2110-2123.

## 7. FIGURE CAPTIONS

1. Examples of MMCR Doppler spectra generated from a) two different phase mode particle size distributions with enough size separation to create a bimodal Doppler spectrum and b) two different phase particle size distributions that do not have sufficient velocity difference to generate a clear bimodal Doppler spectrum separated by noise bins.

2. Synthetic MMCR Doppler spectra generated by a) a single Gaussian distribution, b) the superposition of two equal magnitude Gaussian distributions, c) the superposition of two unequal magnitude Gaussian distributions, and d) through f) their corresponding continuous wavelet transforms.

3. a) The Marr wavelet at each scale used, b) example of an observed mixed-phase Doppler spectrum, and c) the corresponding wavelet transform of the Doppler spectrum at each scale.

4. Measured lidar backscatter cross section versus circular depolarization ratio for most of October 2004 with the region corresponding to liquid detection outlined by a gray box.

5. Illustration of the selection scheme for choosing training data. Training data is sparsely sampled from one-hour time windows every seven hours. The population of training samples is distributed evenly over height. Thus every range gate,  $g_1$ ,  $g_2$ ,  $g_3$ ... $g_n$  contributes roughly the same number of samples.

6. Time-height mapping of MMCR a) radar reflectivity with radiosonde temperature

profile, b) mean Doppler velocity, and c) Doppler spectrum width for a one-hour period (10:00-11:00 UTC) on October 7, 2004.

7. Time-height mapping of a) the observed lidar circular depolarization ratio (CDR) for one-hour period (10:00-11:00 UTC) on October 7, b) the observed lidar backscatter for the same period and c) examples of four MMCR Doppler spectra collected during the same period corresponding to the indicated time-height locations in (b).

8. Time-height mapping of a) the predicted lidar CDR using the corresponding MMCR Doppler spectra for the period 10:00-11:00 UTC on October 7, 2004, b) the predicted lidar backscatter for the same period, with the ceilometer cloud base (black dots) plotted for reference, and c) the predicted area of supercooled liquid detections.

9. Soundings of a) relative humidity and b) temperature at 11 UTC on October 7, 2004.

10. Fig. 10. Time-height mapping of a) the observed lidar circular depolarization ratio (CDR) for one-hour period (06:00-07:00 UTC) on October 7, b) the observed lidar backscatter for the same period and c) the observed MMCR radar reflectivity of the same period, with radiosonde temperature profile. This is a multi-layer cloud arctic case.

11. Time-height mapping of a) the predicted lidar CDR using the corresponding MMCR Doppler spectra for the period 06:00-07:00 UTC on October 7, 2004, b) the predicted lidar backscatter for the same period, with the ceilometer cloud base (black dots) plotted for reference, and c) the predicted area of supercooled liquid detections.

12. Time series of a) ceilometer measured cloud base (gray) and the base of radar retrieved liquid (black), b) ceilometer measured cloud base (gray) and the base of significant radar detections (black), and c) MWR measured liquid water path (gray) and column thickness of the radar retrieved liquid mask (black), in range gates, for October 2004. MWR LWP has a 0.68 correlation with retrieved liquid thickness.

13. a) Reflectivity, b) time-interpolated temperature, and c) time-interpolated relative humidity distributions of the October 2004 radar retrieved liquid mask pixels occurring within 1 hour of a radiosonde launch.

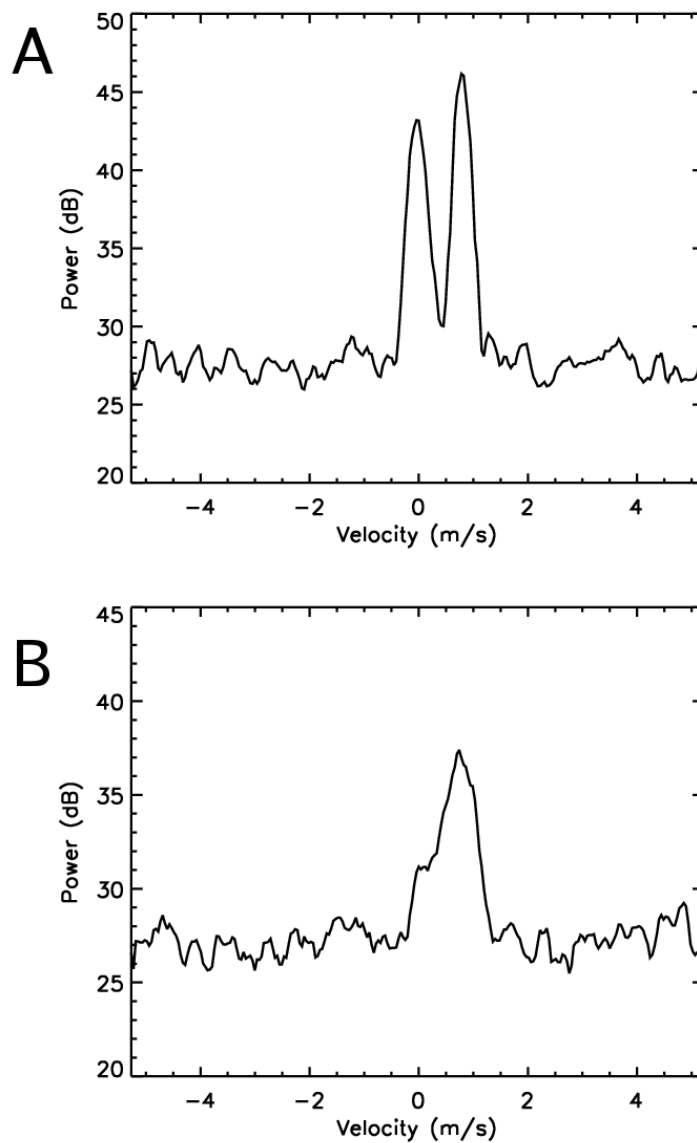


Fig. 1 Examples of MMCR Doppler spectra generated from a) two different phase mode particle size distributions with enough size separation to create a bimodal Doppler spectrum and b) two different phase particle size distributions that do not have sufficient velocity difference to generate a clear bimodal Doppler spectrum separated by noise bins.

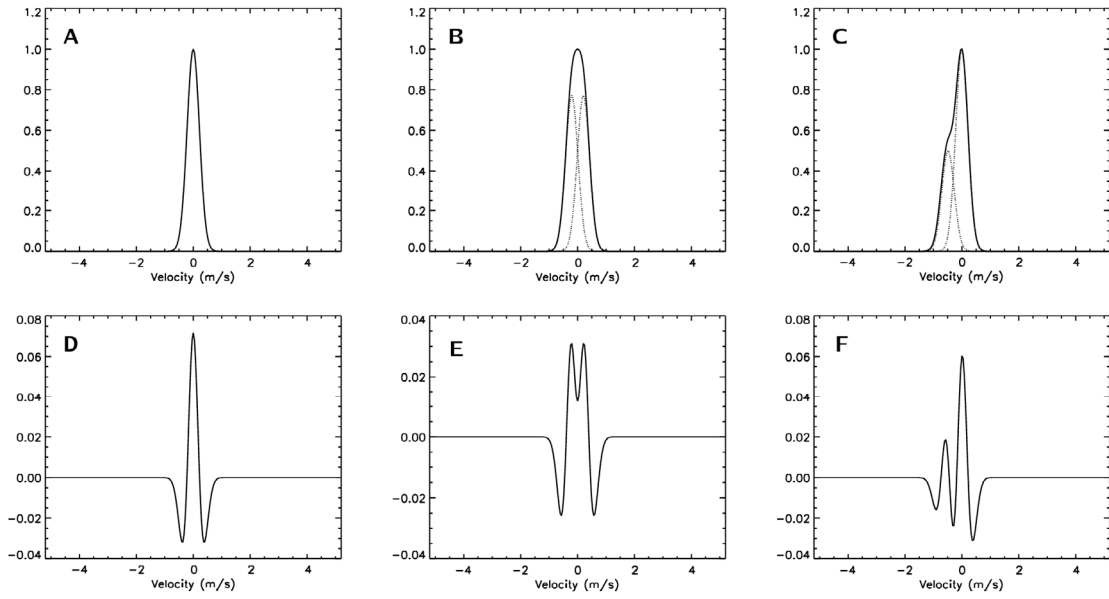


Fig. 2. Synthetic MMCR Doppler spectra generated by a) a single Gaussian distribution, b) the superposition of two equal magnitude Gaussian distributions, c) the superposition of two unequal magnitude Gaussian distributions, and d) through f) their corresponding continuous wavelet transforms.

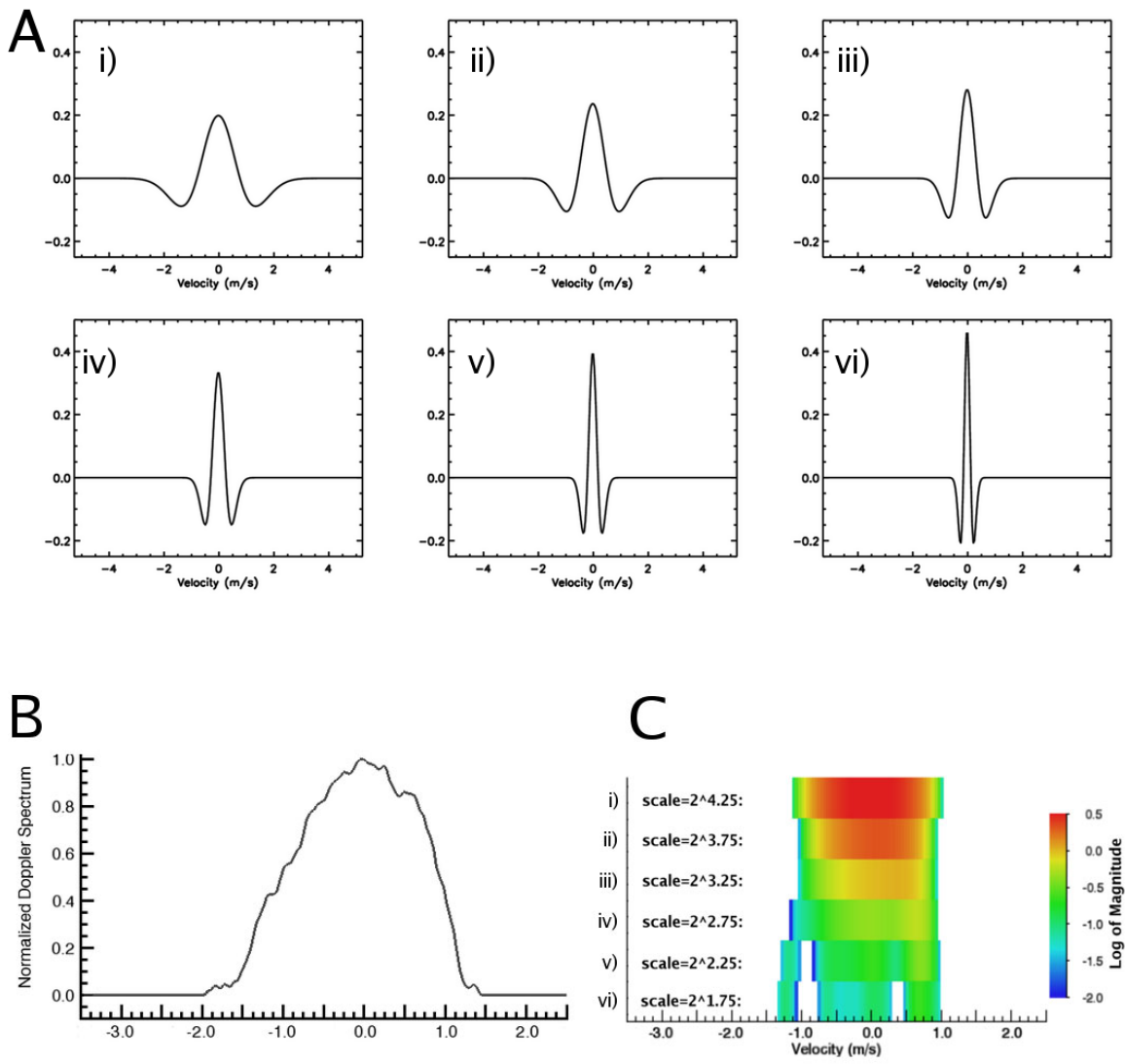


Fig. 3. a) The Marr wavelet at each scale used, b) example of an observed mixed-phase Doppler spectrum, and c) the corresponding wavelet transform of the Doppler spectrum at each scale.

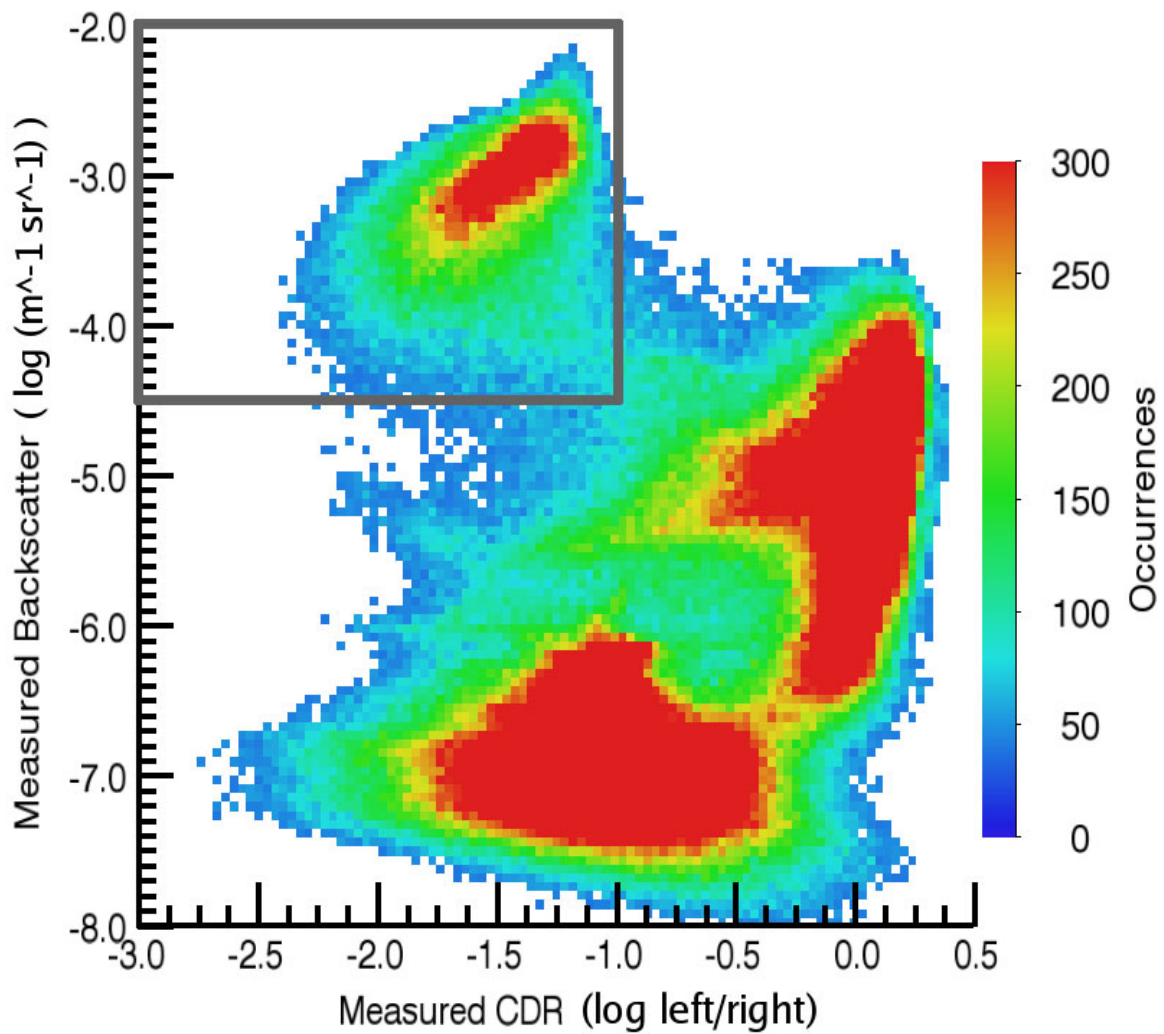


Fig. 4. Measured lidar backscatter cross section versus circular depolarization ratio for most of October 2004 with the region corresponding to liquid detection outlined by a gray box.

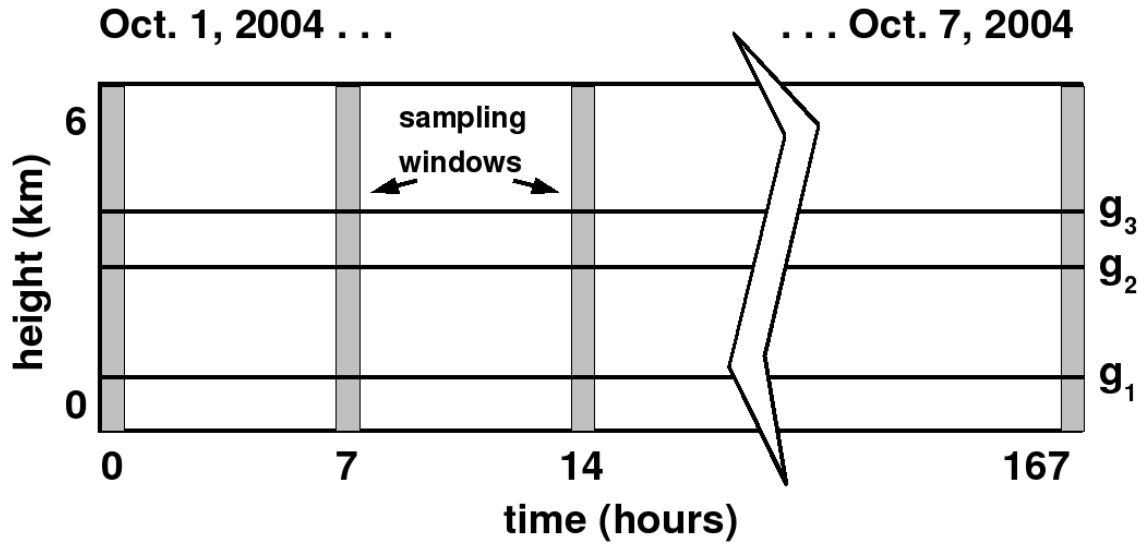


Fig. 5. Illustration of the selection scheme for choosing training data. Training data is sparsely sampled from one-hour time windows every seven hours. The population of training samples is distributed evenly over height. Thus every range gate,  $g_1, g_2, g_3 \dots g_n$  contributes roughly the same number of samples.

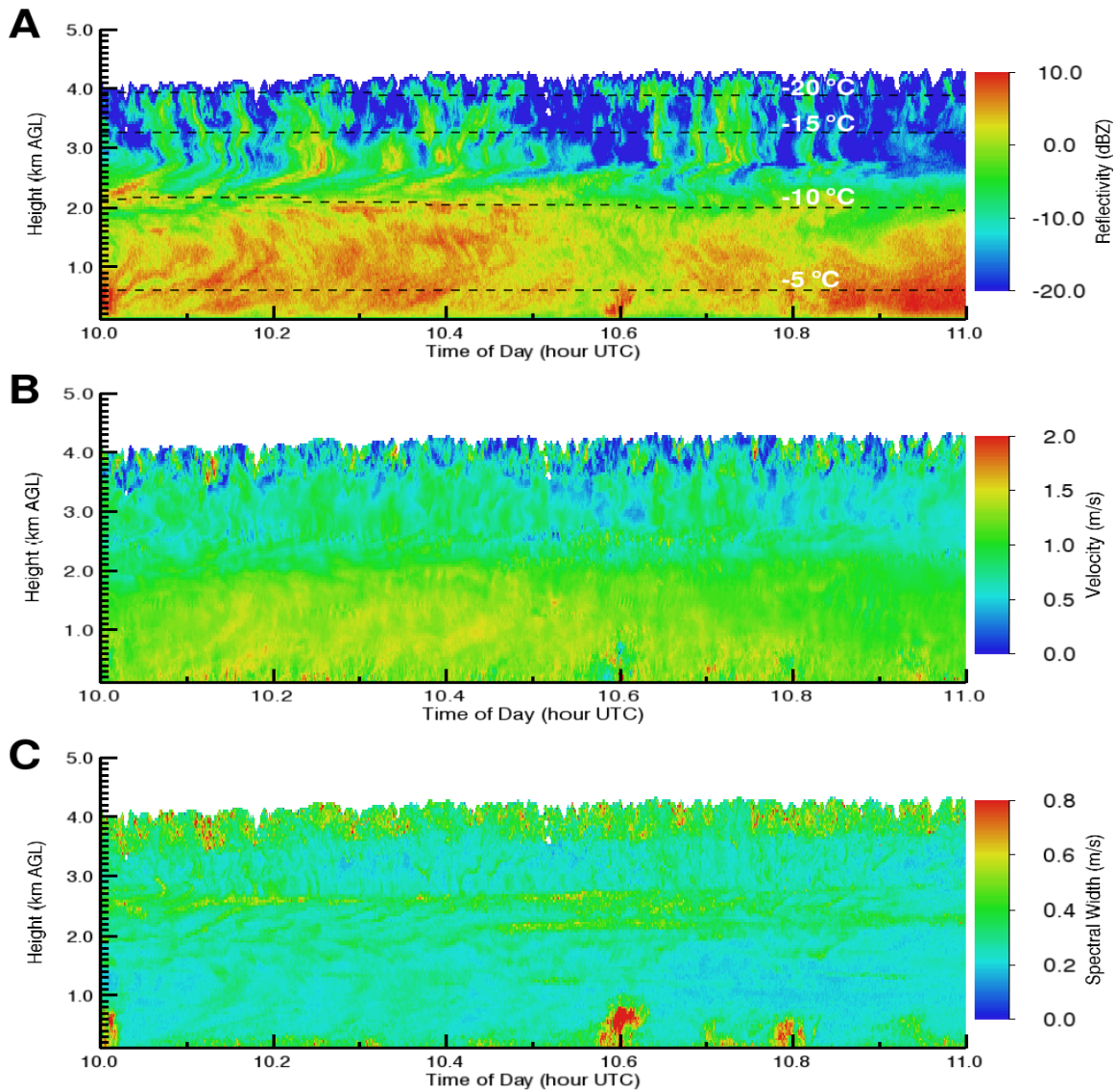


Fig. 6. Time-height mapping of MMCR a) radar reflectivity with radiosonde temperature profile, b) mean Doppler velocity, and c) Doppler spectrum width for a one-hour period (10:00-11:00 UTC) on October 7, 2004.

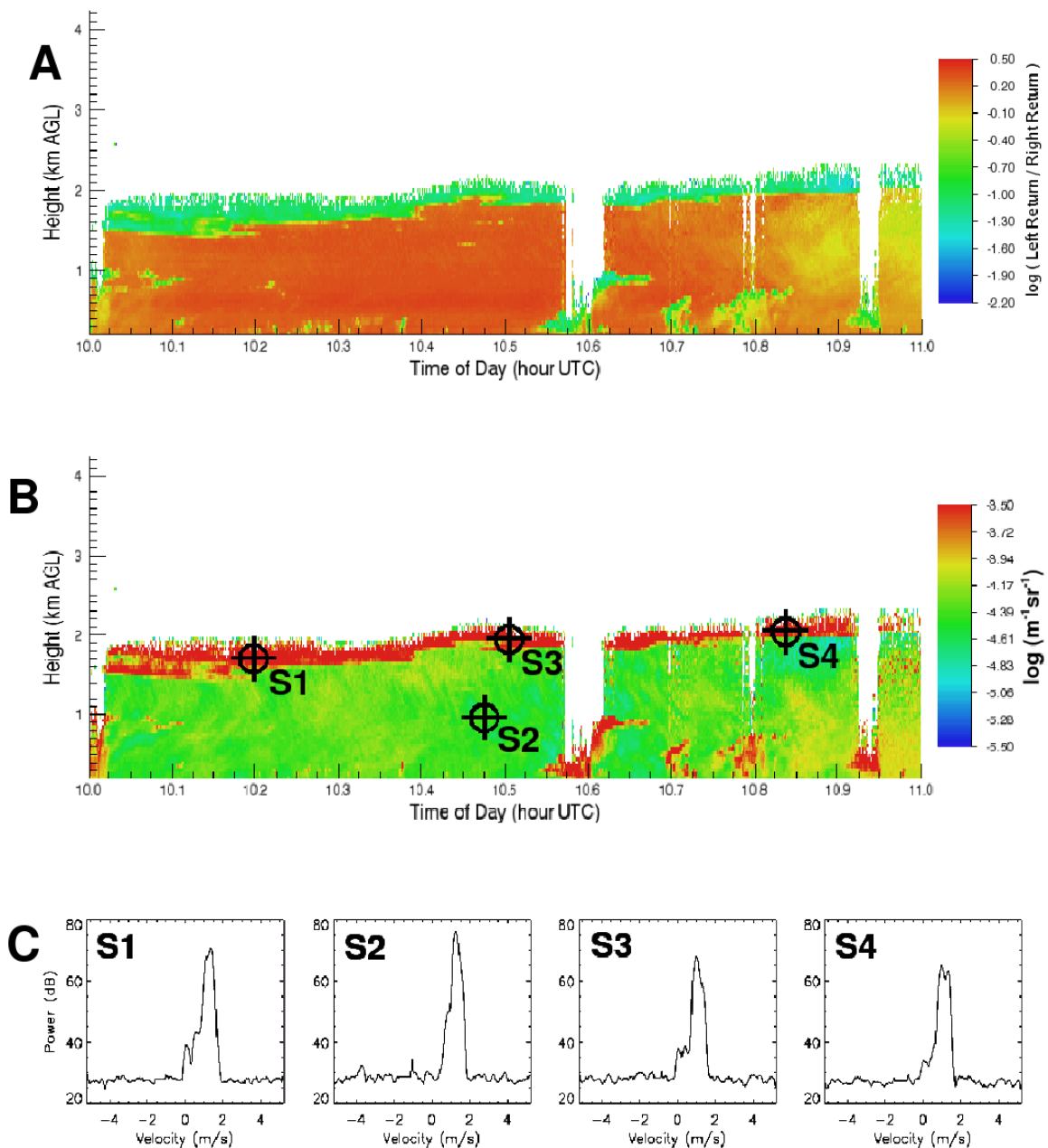


Fig. 7. Time-height mapping of a) the observed lidar circular depolarization ratio (CDR) for one-hour period (10:00-11:00 UTC) on October 7, b) the observed lidar backscatter for the same period and c) examples of four MMCR Doppler spectra collected during the same period corresponding to the indicated time-height locations in (b).

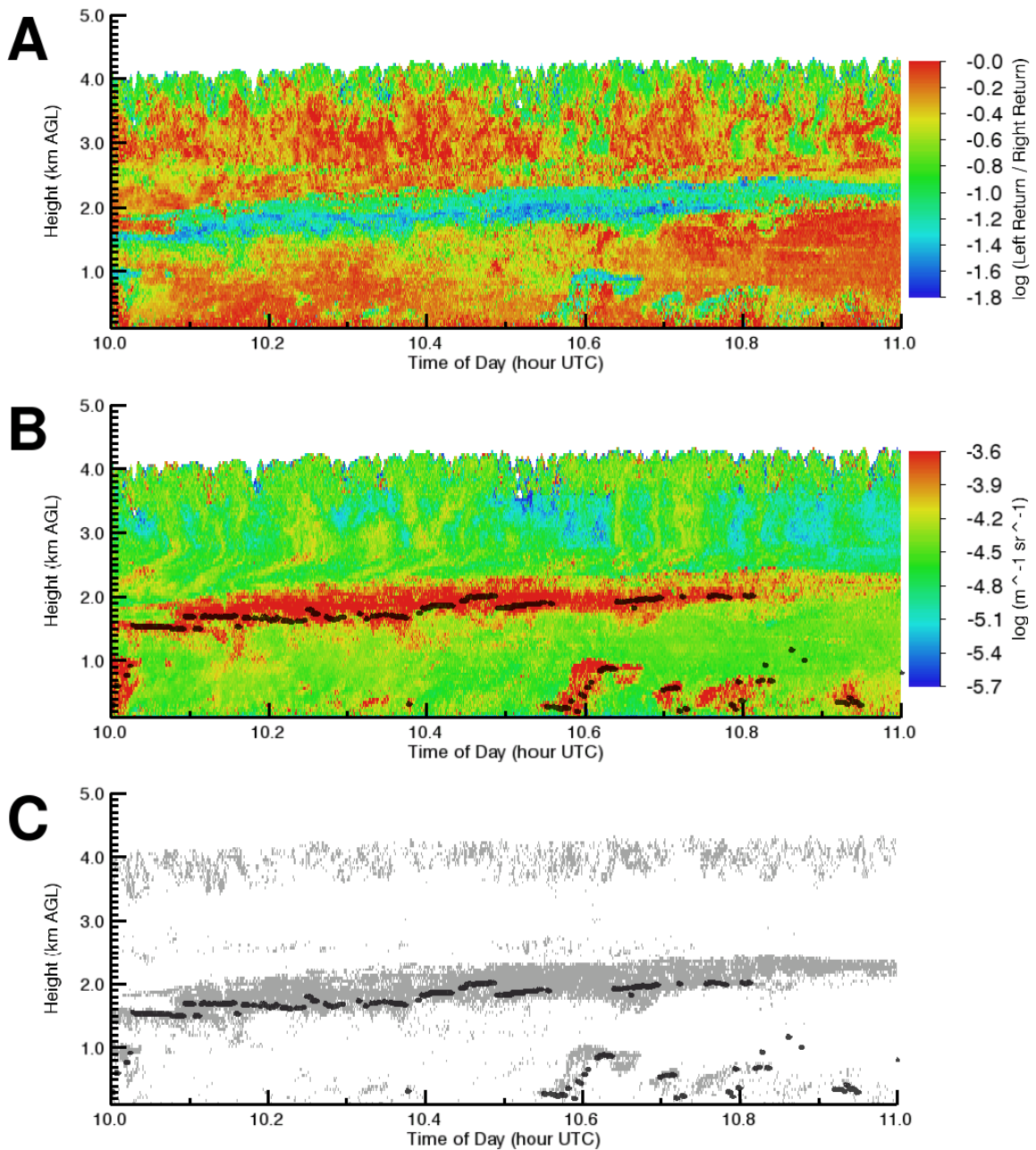


Fig. 8. Time-height mapping of a) the predicted lidar CDR using the corresponding MMCR Doppler spectra for the period 10:00-11:00 UTC on October 7, 2004, b) the predicted lidar backscatter for the same period, with the ceilometer cloud base (black dots) plotted for reference, and c) the predicted area of supercooled liquid detections.

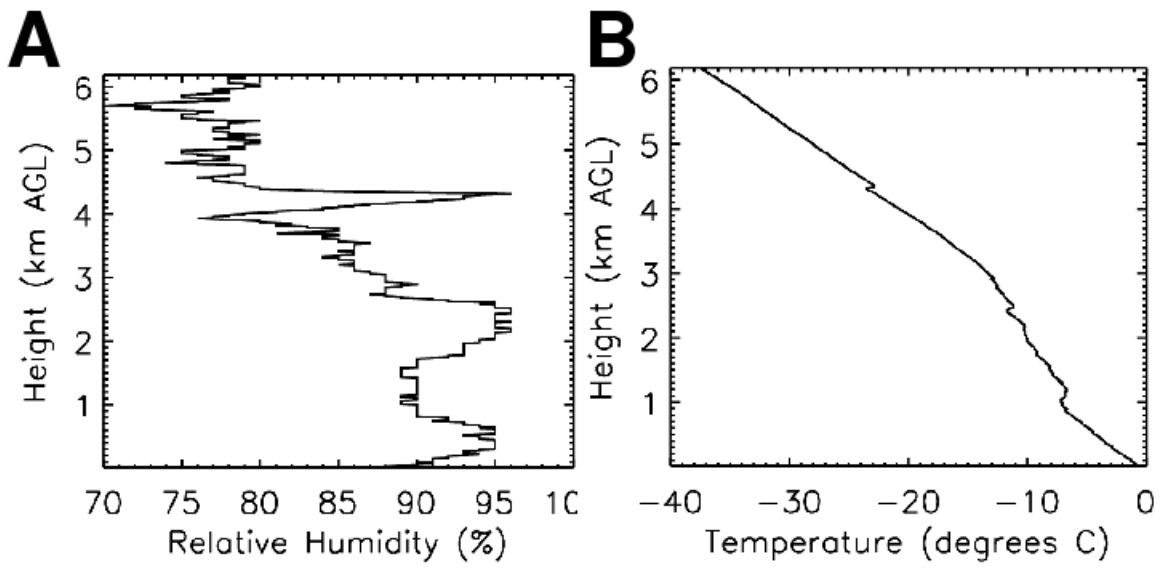


Fig. 9. Soundings of a) relative humidity and b) temperature at 11 UTC on October 7, 2004.

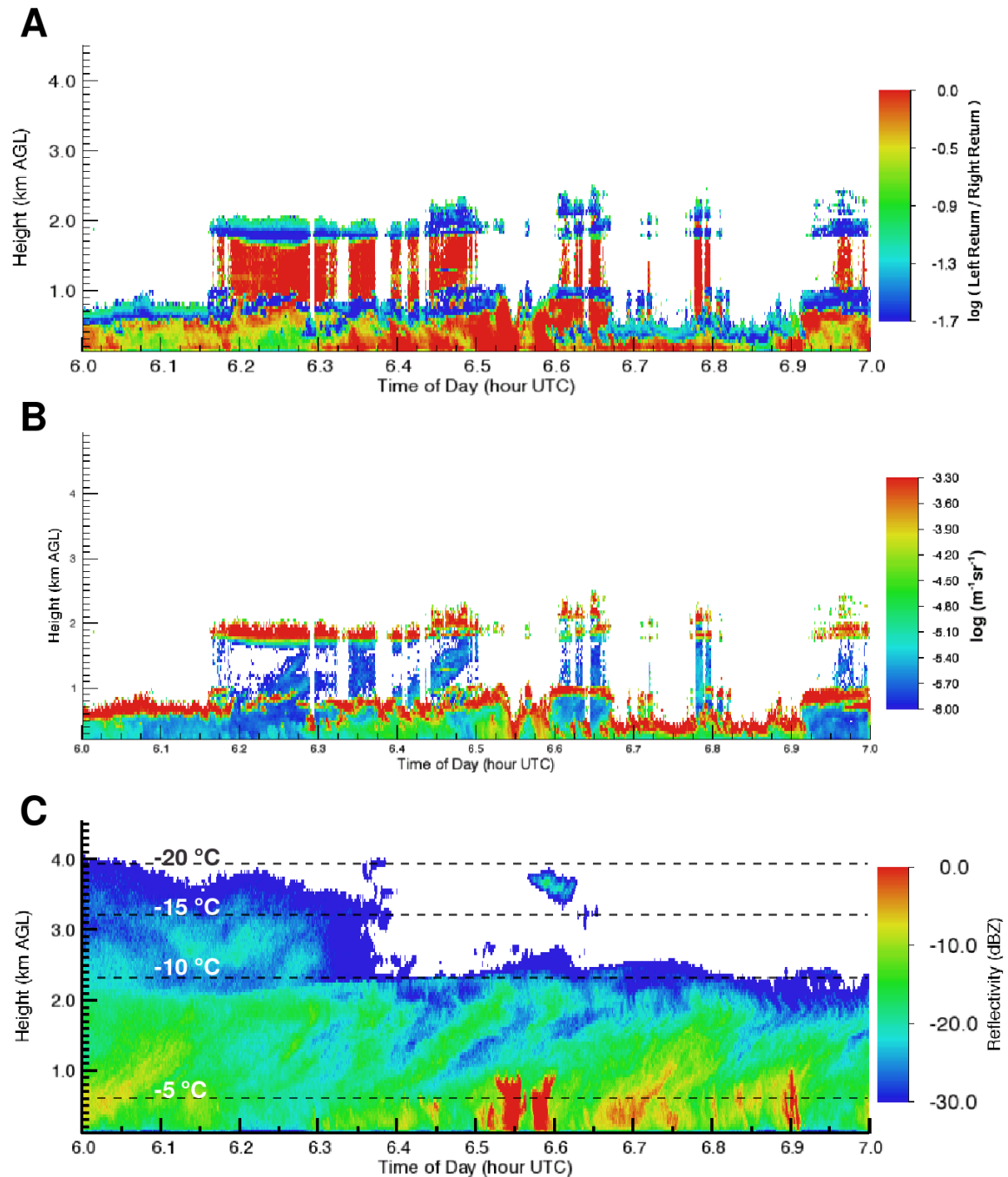


Fig. 10. Time-height mapping of a) the observed lidar circular depolarization ratio (CDR) for one-hour period (06:00-07:00 UTC) on October 7, b) the observed lidar backscatter for the same period and c) the observed MMCR radar reflectivity of the same period, with radiosonde temperature profile. This is a multi-layer cloud arctic case.

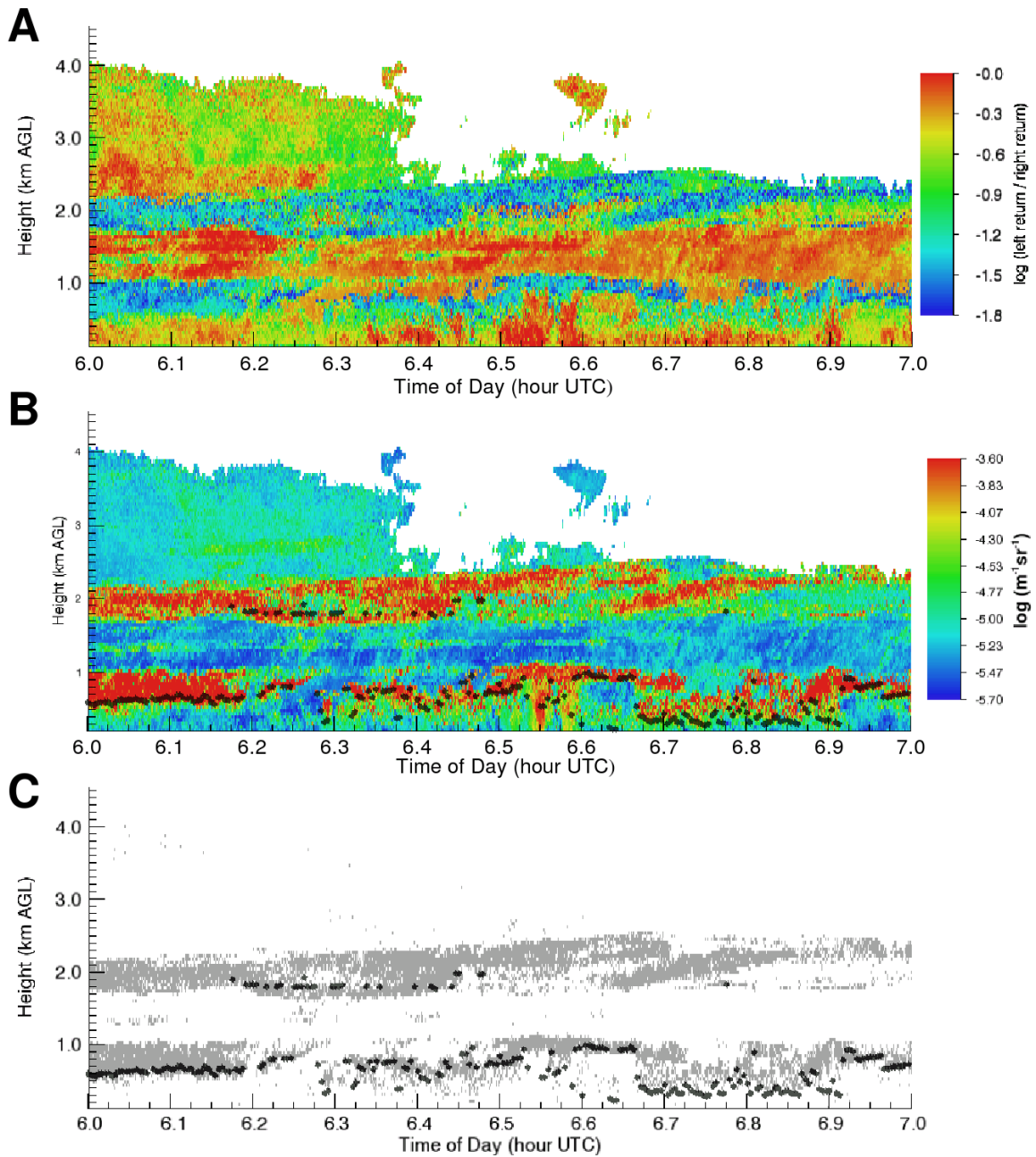


Fig. 11. Time-height mapping of a) the predicted lidar CDR using the corresponding MMCR Doppler spectra for the period 06:00-07:00 UTC on October 7, 2004, b) the predicted lidar backscatter for the same period, with the ceilometer cloud base (black dots) plotted for reference, and c) the predicted area of supercooled liquid detections.

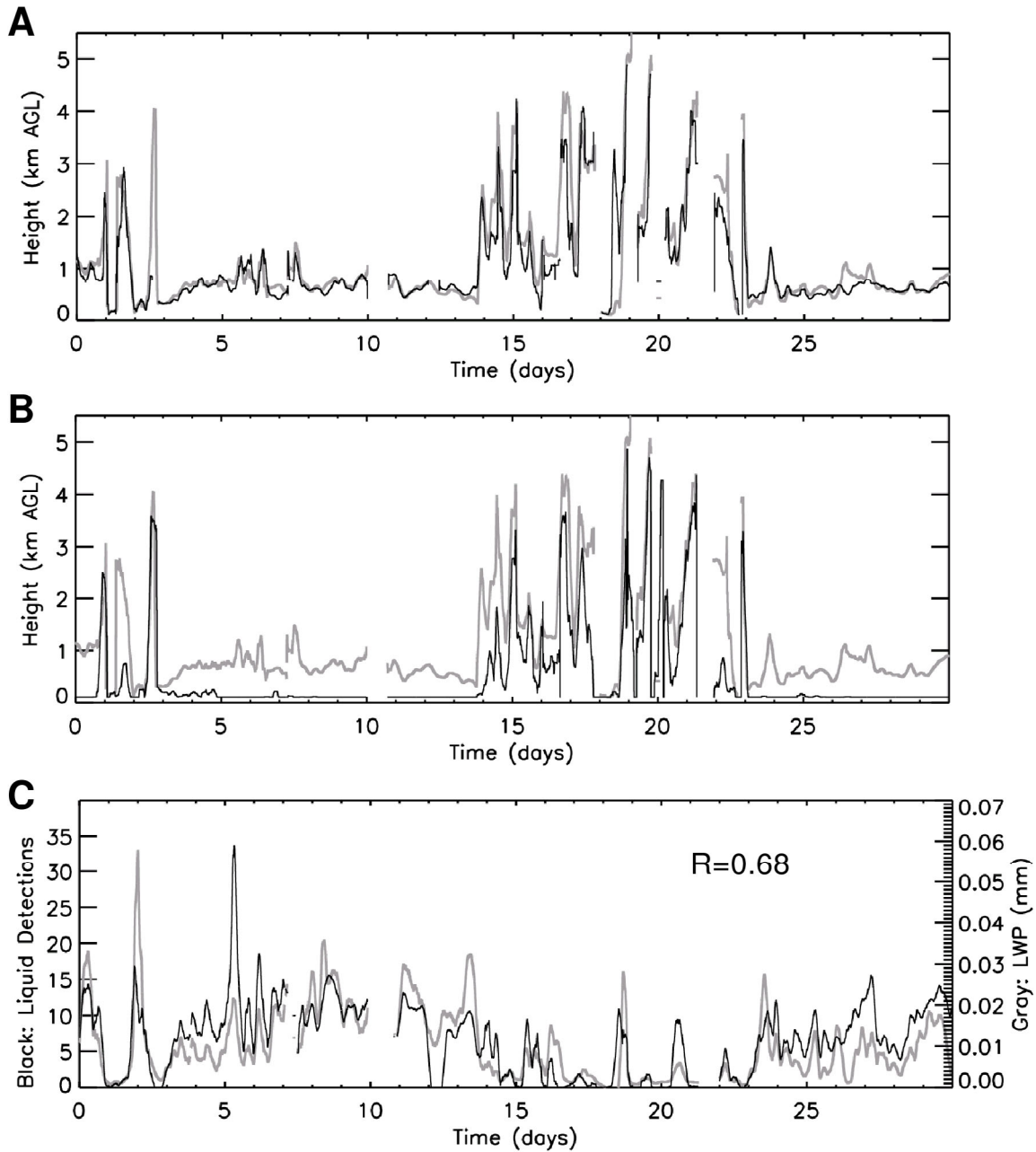


Fig. 12. Time series of a) ceilometer measured cloud base (gray) and the base of radar retrieved liquid (black), b) ceilometer measured cloud base (gray) and the base of significant radar detections (black), and c) MWR measured liquid water path (gray) and column thickness of the radar retrieved liquid mask (black), in range gates, for October 2004. MWR LWP has a 0.68 correlation with retrieved liquid thickness.

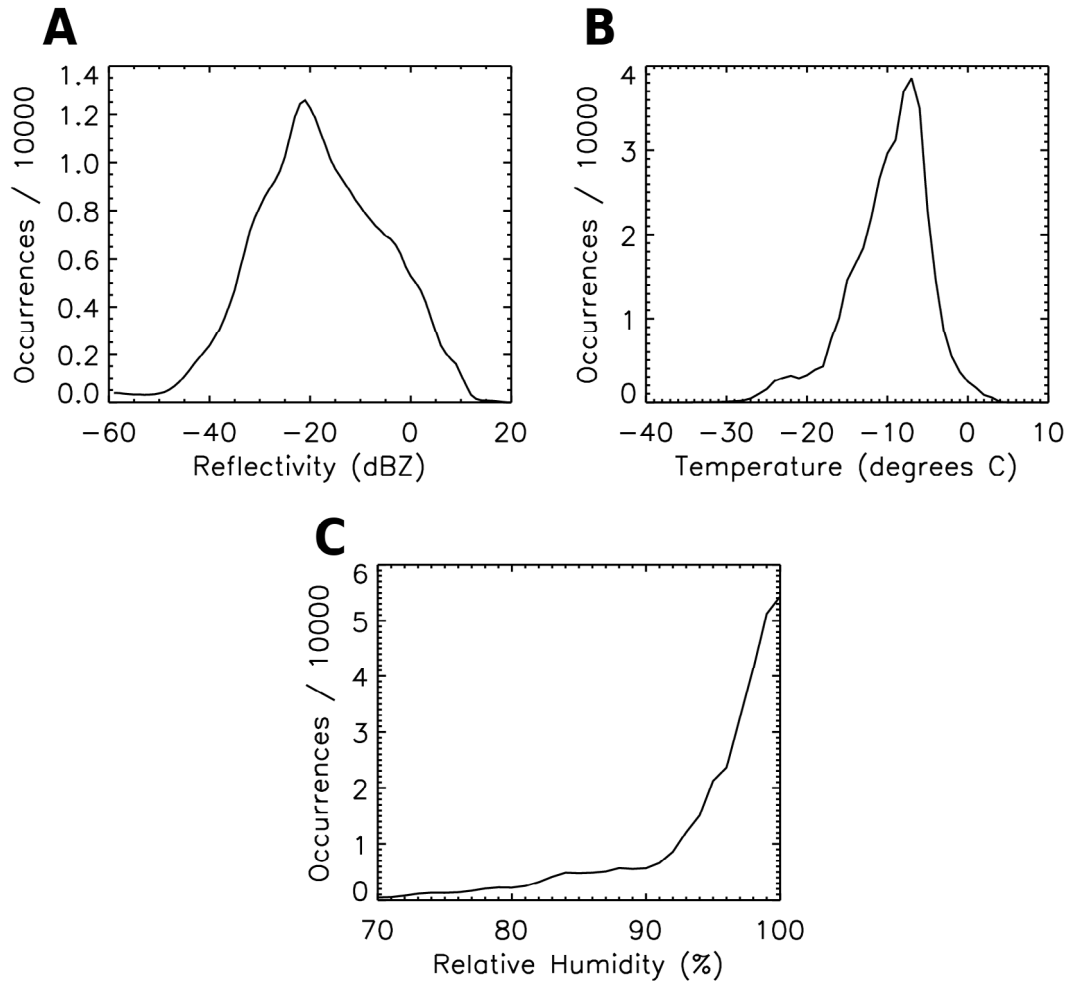


Fig. 13 a) Reflectivity, b) time-interpolated temperature, and c) time-interpolated relative humidity distributions of the October 2004 radar retrieved liquid mask pixels occurring within 1 hour of a radiosonde launch.